Hot corrosion behavior of the spray-formed nickel-based superalloy

Min Xia(夏敏)[1,†], Tian-Fu Gu(谷天赋)[1], Chong-Lin Jia(贾崇林)[1,2], and Chang-Chun Ge(葛昌纯)[1,‡]

[1] *School of Materials Science and Engineering, University of Science and Technology Beijing, Beijing* 100083, *China*
[2] *Science and Technology on Advanced High Temperature Structural Materials Laboratory, Beijing Institute of Aeronautical Materials, Beijing* 100095, *China*

(Received 13 July 2016; revised manuscript received 9 September 2016; published online 25 October 2016)

An investigation of low temperature hot corrosion is carried out on a spray-formed nickel-based superalloy FGH100 pre-coated with Na_2SO_4-NaCl at 700 °C for 100 h. Mass gain measurement, x-ray diffraction, scanning electron microscopy, and energy dispersive x-ray spectroscopy are used to study the corrosion behavior. Results reveal that corrosion behavior follows a sequence, that is, first rapidly proceeding, then gradually slowing down, and finally forming an outer layer composed of different types of oxides and an inner layer mainly comprised of sulfides. In-depth analysis reveals that the hot corrosion of FGH100 is a combined effect of oxidation-sulfidation and transfer of oxides.

Keywords: superalloy, molten salts; hot corrosion, oxidation

PACS: 81.20.Ev, 83.50.Uv, 62.20.–x **DOI:** 10.1088/1674-1056/25/12/128103

1. Introduction

Generally, nickel-based superalloy possesses a good mechanical strength and an oxidation resistance, which makes it a candidate of structural material for high-temperature applications.[1] Nickel-based superalloy components such as heat engine and heat exchanger are very often exposed to aggressive environments, which are likely to contain oxygen and other reactants such as sulfide, chloride and sodium salt, and mechanical stresses simultaneously.[2–5] It has been shown that a condensation layer of alkali metal salt which is generally considered to be a mixture of the salts of Na_2SO_4 and NaCl is often observed on the surface of the superalloy. The existence of such a condensation layer on the superalloy surface could accelerate the oxidation which can considerably damage the service of high-temperature components,[6] which is known as hot corrosion. Studies[7–12] have shown that the interaction between creep or fatigue and hot corrosion could determine the service life of a superalloy at high temperature.

As is well known, nickel-based superalloys are classified into wrought, cast and powder metallurgy (PM) alloys according to the manufacturing routes.[13] For cast and wrought superalloys, especially directionally solidified superalloys, the hot corrosion behavior has been widely studied.[14–18] Some research of the coatings for resistance to hot corrosion of cast superalloys has already made much progress.[19–24] PM superalloys are used in key components for turbine parts of advanced aero-engines. The PM process has solved the problems of severe segregation, non-uniform microstructure, coarse grains and poor hot working property for the high alloying degree in wrought and cast superalloy.[25,26] Spray forming, also known as spray atomization and deposition, is a solidification processing technology, which was recognized as a special powder metallurgy process (a new type of molding process based on the powder metallurgy).[27–29] Spray-formed superalloy has a similar microstructure to the conventional PM superalloy, and it has some advantages of fine-scale microstructure, lower levels of oxygen and short procedure.[30–32] Explorations for performances of the spray-formed materials are in progress.[33,34]

In the present study, isothermal hot corrosion tests at service temperature are conducted to obtain the corrosion kinetics of spray-formed superalloy FGH100. Typically, FGH100 possesses 50%–60% γ' precipitates and the precipitates are mainly composed of a moderate amount of the primary γ' phase with a mean size of approximately 0.4 mm–1.2 mm, a relatively higher amount of the secondary γ' phase with a mean size of approximately 0.2 mm–0.4 mm, and a marginal amount of the fine tertiary γ' phase with a mean size of approximately 30 nm–70 nm. Carbides and carbonitrides are uniformly distributed at grain boundaries. The microstructural development of the corrosion scale and its phase constitutions of oxidation layers are examined. Specimens of the superalloy FGH100 of determined size are pre-coated with Na_2SO_4-NaCl and tested at 700 °C at atmosphere in a furnace. The evolutions of the corrosion scale and subscale microstructure are studied by using electronic balance, scanning electron microscopy (SEM), energy dispersive spectroscopy (EDS) and x-ray diffraction (XRD).

2. Experimental procedure

FGH100 superalloy was prepared by vacuum induction melting and vacuum arc melting methods. Spray forming ex-

†Corresponding author. E-mail: xmdsg@ustb.edu.cn
‡Corresponding author. E-mail: ccge@mater.ustb.edu.cn

© 2016 Chinese Physical Society and IOP Publishing Ltd

periment was performed at University of Bremen on SK-II in Germany (using nitrogen as atomizing gas and then hot isostatic pressed (HIPed) at 1140 °C and 150 MPa for 3 h. Samples in this testing were taken from the steady-state regions of the ingot. The chemical compositions (mass percent, wt%) of the spray-formed FGH100 superalloy are listed in Table 1.

Table 1. Chemical compositions of FGH100 superalloy (in unit wt%).

Ni	Co	Cr	W	Mo	Al	Ti	Nb	Ta	Zr	C	B
Bal.	21.75	12.77	4.12	2.95	3.60	3.54	1.51	1.52	0.03	0.023	0.022

Hot corrosion samples each with a size of about 10 mm (in length) ×10 mm (in width) ×3 mm (in thickness) were first ground by SiC abrasive paper (1000 grid), then ultrasonically cleaned in acetone and ethanol and dried at 100 °C. The 25 wt%NaCl + 75 wt%Na_2SO_4 saturated aqueous solution was sprayed on each surface of different specimens and dried on heated metal plates. The quantity of salt compounds coated on the alloy samples was about 4.0±0.5 mg/cm^2. They were subjected to isothermal hot corrosion in a furnace at a temperature of about 700±1 °C for 1 h, 3 h, 5 h, 10 h, 20 h, 50 h, and 100 h respectively, with a supplement of salt per 10 h. Then samples were air cooled to room temperature and washed in boiling deionized water for 30 min to dissolve the remaining salt. After being dried at 80 °C for 1 h, the mass of specimens was measured. Three specimens were used to obtain the averaged mass change. One kind of corrosion kinetics at 700 °C was determined through the relationship between mass change per unit area and corrosion time. The other one is the relationship between thickness increase and corrosion time. SEM and EDS were employed to investigate the morphologies of cross-section and surface. Phase constitutions of corrosion layers were detected by XRD.

3. Results

3.1. Corrosion kinetics and characterization

Figure 1 shows the isothermal corrosion kinetic curves of samples at 700 °C in NaCl–Na_2SO_4 salts. Figure 1(a) displays the mass change per unit area of specimen with time. It is clear that mass increases rapidly within the first 5 h, then gradually slows down as time goes by. After 100-h exposure, the mass of samples increases up to 12.8 mg/cm^2. Data are calculated by oxidation experience formula of Wagner:[6,13] $M\Delta^n = Kt$, the mass gain of spray-formed FGH100 superalloy in the isothermal corrosion process, where ΔM is the mass gain per unit area, t is the exposure time, n is the corrosion exponent, and K is the corrosion rate constant. specifically, in our case it is in the following form:

$$\Delta M^{1.744} = 1.122t. \quad (1)$$

R-square reaches 0.979, which indicates that there is a certain relationship between the mass increase per unit area and corrosion time. However, the kinetic curve of mass change may not reflect hot corrosion resistance, since the spalling of corrosion products is inevitable in the whole process. In this case, mean thickness data of corrosion layers are collected. Variations of the thickness of the outer layer (the oxides growing on the surface) and inner layer (the affected part of the substrate), and the variation of the total corrosion scale with time are presented in Fig. 1(b). The data plotted are the averaged (equally spaced) measurements of the inner and outer layers, and overall scale thickness for each test condition. It is this combination of them that could help us achieve the overall situation. The outer layer is slightly thicker than the inner layer in general. The growth of the layer exhibited approximates the kinetic of mass change that there is a steep gradient at the initial stage, and the growth slows down later.

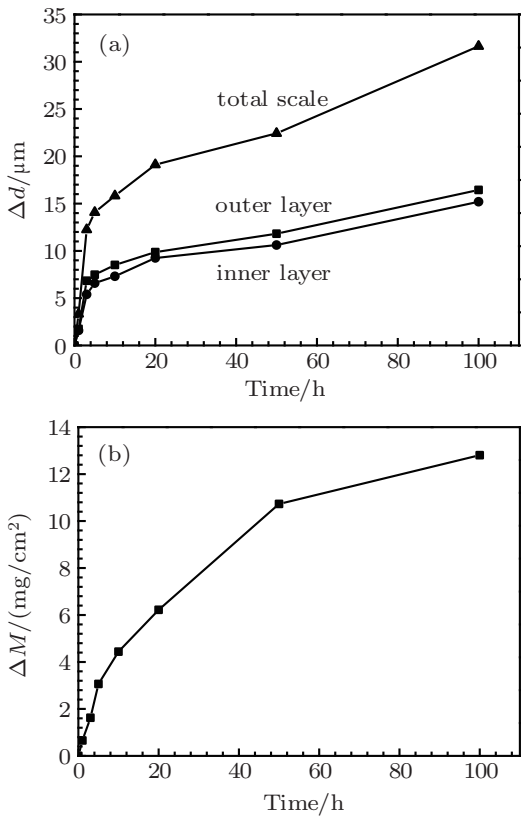


Fig. 1. Plots of (a) mass change and (b) thickness of the corrosion layer for spray-formed FGH100 tested at 700 °C in air versus exposure time.

3.2. Phase constitution and surface morphology of corrosion layer

Figure 2 shows the XRD patterns of the surface corrosion products on the surfaces of the specimens after the corrosion tests at 700 °C for 1 h, 10 h, and 100 h, respectively. The initial corrosion products formed on the surface of the specimens are NiO and tiny CoO. After hot corrosion of 10h, $CoAl_2O_4$, $NiAl_2O_4$, and $NiCr_2O_4$ with spinel structure are detected. When testing for 100 h, the XRD data are the same as those for 10 h. XRD results are in good agreement with the corrosion kinetics in Fig. 1. However, little amount of sulfide is found.

Figure 3 shows the surface morphologies of spray-formed superalloy FGH100 after hot corrosion and EDS analysis results of the corrosion products. Oxide particles are observed to have a variety of shapes, including clusters, granulars and rods, as shown in Figs. 3(a), 3(c), and 3(e). These surface corrosion products contain a large amount of Cr, Co, Ni, O, and a small amount of Ti and Al. It can be seen that none of these surface layers have a compact and uniform structure. Some cracks are observed on the surface of the outer layer.

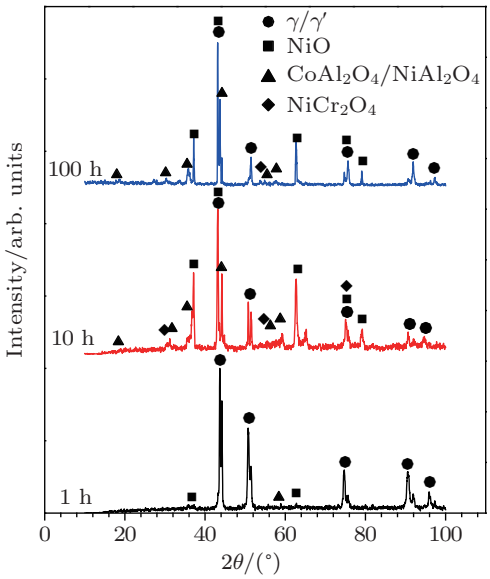


Fig. 2. (color online) XRD patterns of the surface corrosion products of spray-formed FGH100, tested at 700 °C for 1 h and 10 h, 100 h.

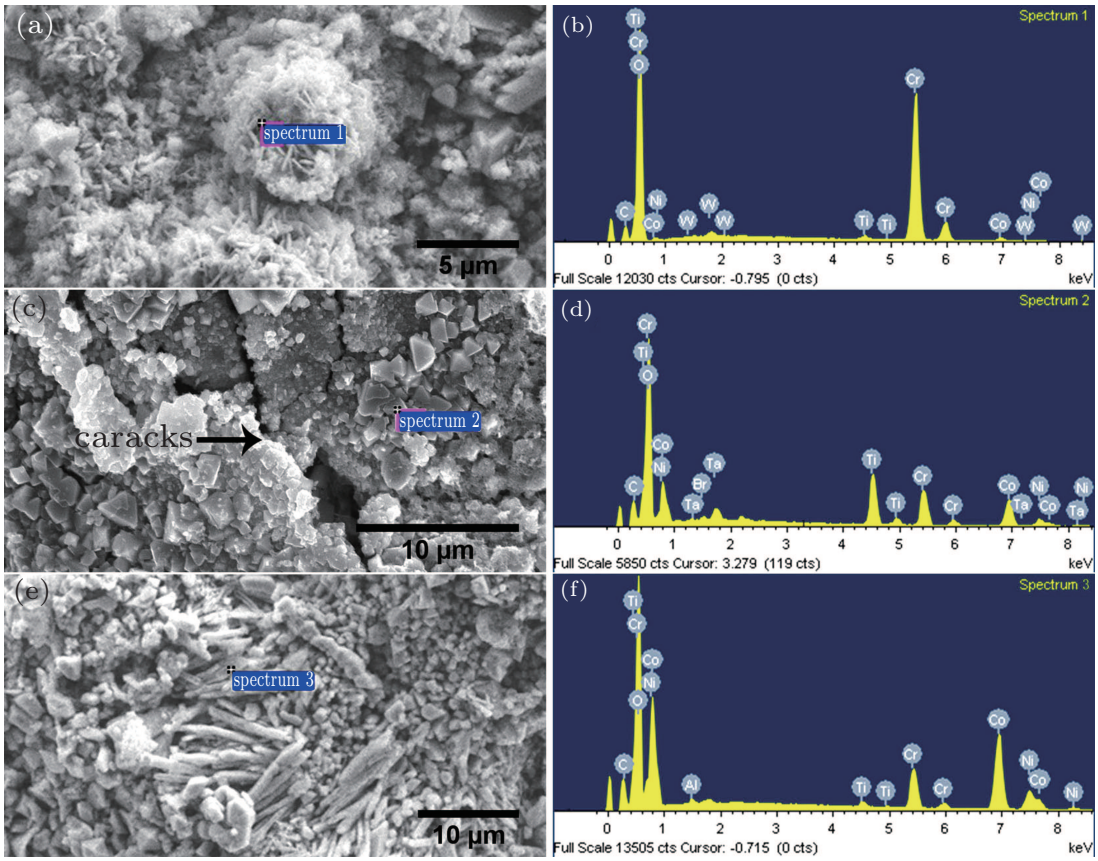


Fig. 3. (color online) Microstructures and EDS analyses of the surface corrosion products of spray-formed FGH100 tested for 100 h: ((a), (c), and (e)) the surface appearance of corroded samples; ((b), (d), and (f)) EDS result of the corrosion products in panels (a), (c), and (e) respectively.

3.3. Cross-sectional morphologies

The cross-sectional morphology can not only describe the structure and thickness of corrosion layer but also reveal the severity and mechanism of hot corrosion attack. Figure 4(a) shows a secondary electron cross-sectional image of the sample after hot corrosion for 100 h. As can be seen, two distinct layers on the substrate are observed (identified as outer and inner

layers). An extraordinary feature of the cross-section morphology is that the natural marker between the two layers is flat and sharp, especially for longer time corrosion. Furthermore, there exists an obvious crack between the outer and inner corrosion layer. It should be detected that the closer to the free surface, the looser the structure of the outer layer tends to be, and some tiny cracks cross the outer corrosion layer, while in the inner corrosion layer some micropores appear instead of the micro cracks. The nearly spherical γ' precipitate is still partially visible in the inner corrosion layer. The presence of the residual γ' phase that has been corroded expressly indicates a slower corrosion rate for these particles than the γ matrix. The composition contrast of the cross-section can be examined by backscattered electron imaging in the SEM as shown in Fig. 4(b), so that the thickness of the inner corrosion could be more precise.

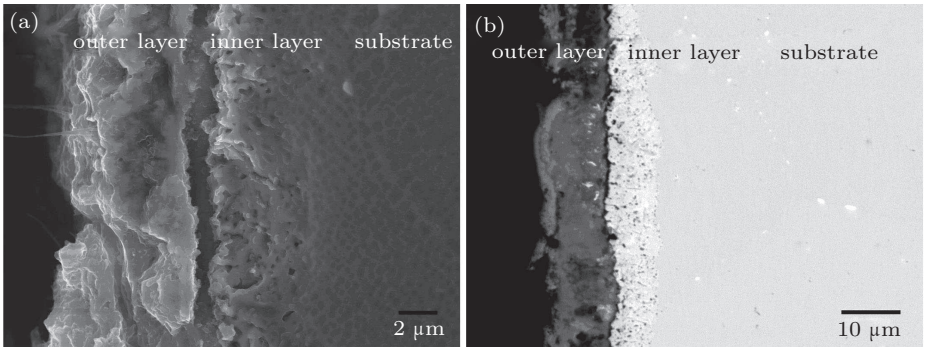


Fig. 4. Cross-sectional morphologies of spray-formed FGH100 tested for 100 h: (a) secondary electron imaging and (b) backscattered electron imaging.

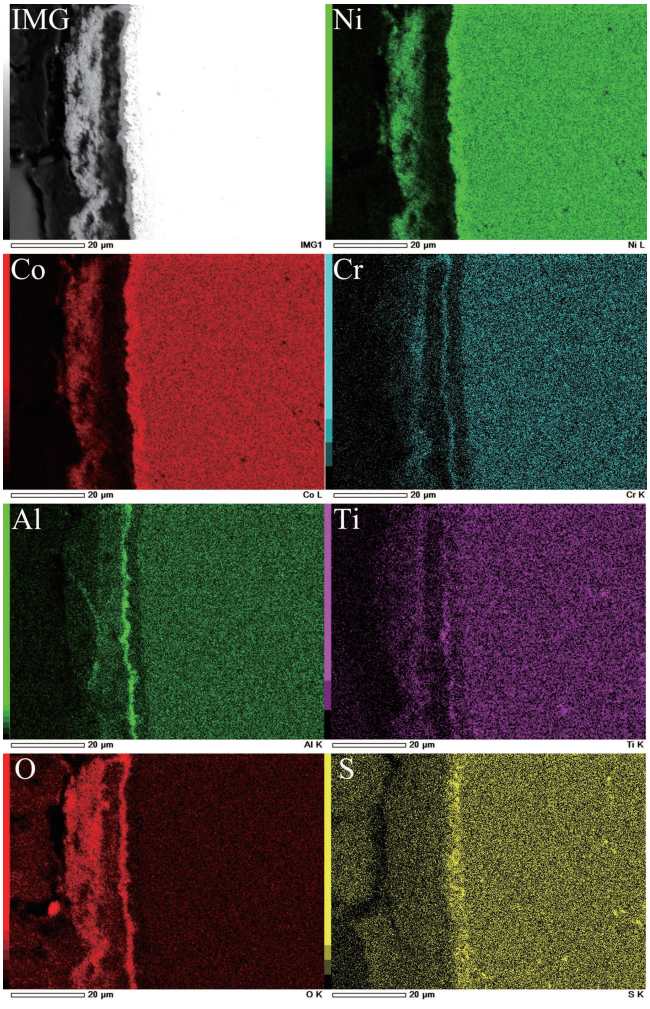


Fig. 5. (color online) Cross-sectional SEM images of spray-formed FGH100 tested for 100 h and the corresponding EDS maps for Ni, Co, Cr, Al, Ti, W, O, and S.

In order to evaluate element distribution, element maps are analyzed by SEM and EDS as shown in Fig. 5. The results of EDS mapping suggest that the outer layer has a component gradient. The part next to the free surface mainly consists of Ni- and Co-based oxides, and the major elements of the inner part are these elements with high oxidation activity such as Cr, Al, and Ti. Also, there is a wide transition zone, in which are formed the $NiCr_2O_4$, $CoAl_2O_4$, $NiAl_2O_4$ with spinel structure and $NiTiO_3$ with perovskite structure. In the inner layer, there is a lack of oxides and S is concentrated. The Ni and Co are more effective than Cr, Al, and Ti to react with S.

From the above results, it is verified that the hot corrosion behavior of spray-formed superalloy FGH100 is controlled by the element diffusion. In this paper, further analysis and discussion are conducted to obtain the concrete mechanism.

4. Discussion

There are two temperature-dependent regimes of hot corrosion as observed by peaks in corrosion rate curve, which are more aggressive than air exposure alone. The two corrosion rate peaks occur at 900 °C–1000 °C and 600 °C–750 °C. The high-temperature hot corrosion which proceeds at 900 °C–1000 °C is associated with the melting point of Na_2SO_4 (Tm = 884 °C). This study focuses on the low-temperature hot corrosion (at 600 °C∼750 °C), in which molten $Na_2SO_4 + NaCl$ eutectic (630 °C) forms that acts to lower the liquidus temperature. Because of the molten $Na_2SO_4 + NaCl$ eutectic temperature (630 °C), the corrosion behavior appears in the liquid phase.[35] Based on the experimental results and theories,[13,36–38] the hot corrosion mech-

anism of the spray-formed superalloy FGH100 is gradually clear.

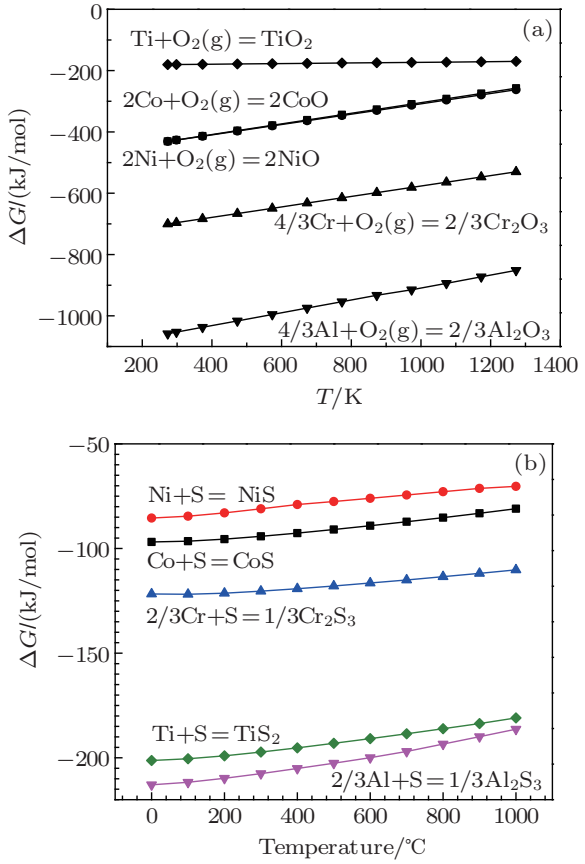


Fig. 6. (color online) Gibbs free energies for (a) oxidation and (b) sulfuration of alloying elements in a temperature range from 0 °C to 1000 °C.

The participation levels of alloying elements in hot corrosion are different, which depends on the content of a certain element and the free energy of oxidation or sulfuration.[39] The standard Gibbs free energies for oxidation and sulfuration are shown in Fig. 6, which are calculated by HSC Chemistry Software. The free energies of formation for Ni, Co, Cr Al, and Ti oxides are more negative than those of their corresponding sulfides.

In the beginning of the reaction with the molten salt, the nickel- and Co-rich γ-matrix appeared to be the first phase dissolved:

$$4\mathrm{M} + \mathrm{SO_4^{2-}} = \mathrm{MS} + 3\mathrm{MO} + \mathrm{O^{2-}}. \quad (2)$$

It is a general and common reaction. With the generations of MS and MO, the activity of $\mathrm{O^{2-}}$ near the reaction interface increases, so that the chemical reaction below occurs:

$$\mathrm{MO} + \mathrm{O^{2-}} = \mathrm{MO_2^{2-}}. \quad (3)$$

The resulting products can diffuse to the free surface of molten salt and decompose for the lower activity of $\mathrm{O^{2-}}$ there. The decomposition products MO form a loose oxidation layer without any protectiveness. The MS will be left in the interface. Because Cr is also a major element in γ-matrix, the formation of $\mathrm{Cr_2O_3}$ is the next only to NiO and CoO. What is more, the $\mathrm{Cr_2O_3}$ has the priority to combine with the $\mathrm{O^{2-}}$ through the following reaction

$$\mathrm{Cr_2O_3} + \mathrm{O^{2-}} + 3/2\mathrm{O_2} = 2\mathrm{CrO_4^{2-}}. \quad (4)$$

The reaction consumes amounts of $\mathrm{O^{2-}}$, which will not only inhibit the dissolutions of NiO and CoO but also accelerate the decomposition of $\mathrm{NiO_2^{2-}}$ and $\mathrm{CoO_2^{2-}}$ near the free surface. After that, the Cr taking part in the reaction would exist in the form of radical ions due to its high stability until it reaches saturation point in the liquid phase. For this reason, there will be sufficient time to form a $\mathrm{Cr_2O_3}$ layer with continuous structure, which is the key to further preventing the layer from being corroded. The precipitation of $\mathrm{Cr_2O_3}$, of course, has a tendency to be close to the outside surface for the gradient of $\mathrm{O^{2-}}$ activity. Although the relatively stable γ' precipitates are secondary, it will suffer partial or incomplete dissolving, bringing Al and Ti into this corrosion process. As with the NiO and CoO, the oxides of Al and Ti would be deposited in the vicinity of the free surface after dissolving in superalloy-melt interface as a result of the role of the gradient. However, the oxide films of Al and Ti are also non-compact and non-protective. The constant consumption of $\mathrm{SO_4^{2-}}$ in the process of corrosion suggests that the progress should stop if the supplement were little.

Although $\mathrm{Na_2SO_4}$ is dominant, it is proven beyond doubt that the addition of even small amounts of NaCl in $\mathrm{Na_2SO_4}$ is much more harmful than only either NaCl or $\mathrm{Na_2SO_4}$.[40] The oxidation layers containing $\mathrm{Cr_2O_3}$ and $\mathrm{TiO_2}$ are sensitive to $\mathrm{Cl^-}$ attack, leaving behind a porous structure. What is more, NaCl contamination can easily induce extensive spalling.[39]

According to the negative Gibbs free energies from 0 °C to 1000 °C shown in Fig. 7, the spinels and perovskites are formed from NiO, CoO, $\mathrm{Cr_2O_3}$, $\mathrm{Al_2O_3}$, and $\mathrm{TiO_2}$ spontaneously, thus providing theoretical bases for understanding the occurrences of these composite oxides. It is a process of self-diffusion and mutual-diffusion.

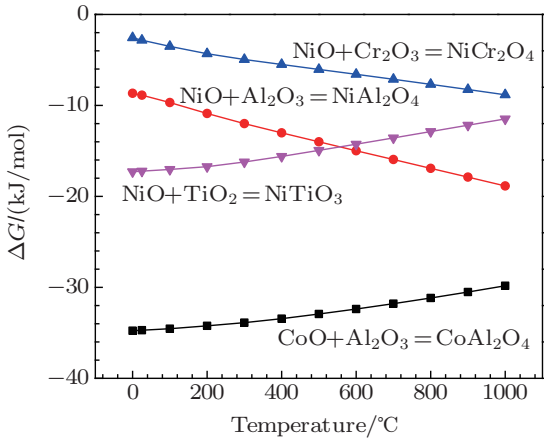


Fig. 7. (color online) Gibbs free energies for combination reactions of these simple metal oxides from 0 °C to 1000 °C.

In the course of its development, the gradient of O^{2-} activity is an extremely critical factor, which gives rise to the "uphill" diffusion, interactive permeation among components and the formation of protective or non- protective oxide layers.[15]

Atomic diffusion could conduce to variation of vacancy concentration, so that the appearance of a porous structure in the inner corrosion layers is because of the on-going vacancy clustering and growing with the increase of oxidation time. The crack between the outer and inner layers is left for the dissolving of sodium salt nearest to the inner layer.

As a summary of the above analysis, it is proposed that corrosion behavior of the spray-formed FGH100 could be divided into two parts: oxidation-sulfuration and transfer of oxides. The former is the foundation of the latter, and the latter determines the difference between hot corrosion and conventional oxidation. A close connection exists between the two. Ultimately, the oxidation-sulfuration process, as well as the concurrent evolution of the diffusion structure of the corrosion scale in low-temperature hot corrosion examined in this study, may be better appreciated in the framework of multi-component hot corrosion phenomenology on the basis of corrosion kinetics and compositional distributions for various components.

5. Conclusions

During hot corrosion, the sample mass and layer depth increase with time going by at service temperature. The outer compositions of hot-corroded superalloy FGH100 surface are composed of NiO, $CoAl_2O_4$, $NiAl_2O_4$, and $NiCr_2O_4$, while the inner compositions are mainly sulfides and the residual substrate. Hot corrosion of spray-formed superalloy FGH100 is confirmed to be a combination effect of oxidation-sulfidation and transfer of oxides.

References

[1] Chen G L 1988 *Superalloy* (Beijing: Metallurgical Industry Press)
[2] Zhang K, Liu M M, Liu S L, Sun C and Wang F H 2011 *Corros. Sci.* **53** 1990
[3] Kai W, Lee C H, Lee T W and Wu C H 2001 *Oxid. Met.* **56** 51
[4] Lv J X, Zheng L, Zhang M C and Dong J X 2009 *Acta Metall. Sin.* **45** 204
[5] Deb D, Iyer S R and Radhakrishnan V M 1996 *Mater. Lett.* **29** 19
[6] Zheng L, Zhang M C and Dong J X 2011 *Mater. Design* **32** 1981
[7] Yang X, Li S and Qi H 2015 *Int. J. Fatigue.* **70** 106
[8] Sahu J K, Gupta R K, Swaminathan J, Paulose N and Mannan S L 2013 *Int. J. Fatigue.* **51** 68
[9] Pieraggi B 1987 *Mater. Sci. Eng.* **88** 199
[10] Sahu J K, Ravi Kumar B, Das S K, Paulose N and Mannan S L 2015 *Mater. Sci. Eng. A* **622** 131
[11] Hou J S, Zhou L Z, Yuan C, Guo J T, Wang W, Qin X Z and Liaw P K 2013 *Mater. Charact.* **77** 47
[12] Chateau E and Rémy L 2010 *Mater. Sci. Eng. A* **527** 1655
[13] Guo J T 2008 *Mater Science and Engineering for Superalloy* (Beijing: Science Press)
[14] Han F F, Chang J X, Li H, Lou L H and Zhang J 2015 *J. Alloy Compd.* **619** 102
[15] Lortrakul P, Trice R W, Trumble K P and Dayananda M A 2014 *Corros. Sci.* **80** 408
[16] Liu E, Zheng Z, Guan X, Tong J, Ning L and Yu Y I 2010 *J. Mater. Sci. Technol.* **26** 895
[17] Liu G M, Yu F, Tian J H and Ma J H 2008 *Mater. Sci. Eng. A* **496** 40
[18] Cho S, Hur J, Seo C, Yoon J and Park S 2009 *J. Alloy Compd.* **468** 263
[19] Liu Z, Zhao X and Zhou C 2014 *Corros. Sci.* **92** 148
[20] Fan Q X, Jiang S M, Yu H J, Gong J and Sun C 2014 *Appl. Surf. Sci.* **311** 214
[21] Bai C, Luo Y and Koo C 2004 *Surf. Coat. Tech.* **183** 74
[22] Zheng D, Zhu S and Wang F 2006 *Surf. Coat. Tech.* **200** 5931
[23] Ma J, Jiang S M, Gong J and Sun C 2012 *Corros. Sci.* **58** 251
[24] Shirvani K, Saremi M, Nishikata A and Tsuru T 2003 *Corros. Sci.* **45** 1011
[25] Zhang Y W and Shangguan Y H 2004 *Powder Metall. Ind.* pp. 30–43
[26] Pollock T M and Tin S 2006 *J. Propul. Power.* **22** 361
[27] Zhang J S, Xiong B Q and Cui H 2008 *Spray forming rapid solidification technology: principles and applications* (Beijing: Science Press)
[28] Huang P Y, Jin Z P and Chen Z H 2010 *Basic theory and new technology of powder metallurgy* (Beijing: Science Press)
[29] Lavernia E J and Grant N J 1988 *Mater. Sci. Eng. A* **98** 381
[30] Grant P S 1995 *Prog. Mater. Sci.* **4** 497
[31] Yang Y and Hannula S 2008 *Mater. Sci. Eng. A* **477** 63
[32] Zhang Y, Ge C C, Sheng W P and Qiu C J 2012 *Acta Phys. Sin.* **61** 355 (in Chinese)
[33] Guo B, Sun C S, Zhang S C and Ge C C 2013 *Rare Metals.* **32** 347
[34] Xu Y, Shu Q S, Zhang Y and Ge C C 2012 *Mater. Sci. Technol.* **20** 41
[35] Li T F 2003 *High Temperature Oxidation and Hot Corrosion of Metals* (Beijing: Chemical Industry Press)
[36] Zhu R Z, He Y D and Qi H B 1995 *High Temperature Corrosion and High Temperature Corrosion Resistant Materials* (Shanghai: Shanghai Scientific and Technical Publication)
[37] Li M S 2001 *High Temperature Corrosion of Metals* (Beijing: Metallurgical Industry Press)
[38] Rapp R A 2002 *Corros. Sci.* **44** 209
[39] Bourhis Y and John C S 1975 *Oxid. Met.* **9** 507
[40] Kameswari S 1986 *Oxid. Met.* **26** 33